Psychoradiology, 2022, **2**, 156–170
DOI: 10.1093/psyrad/kkac019
Advance access publication date: 28 November 2022
Review

Radiological biomarkers of idiopathic normal pressure hydrocephalus: new approaches for detecting concomitant Alzheimer's disease and predicting prognosis

Hanlin Cai[1,#], Yinxi Zou[1,#], Hui Gao[1], Keru Huang[2], Yu Liu[2], Yuting Cheng[1], Yi Liu[2], Liangxue Zhou[2], Dong Zhou[1] and Qin Chen[1,*]

[1]Department of Neurology, West China Hospital of Sichuan University, Chengdu, Sichuan 610041, China
[2]Department of Neurosurgery, West China Hospital of Sichuan University, Chengdu, Sichuan 610041, China
*Correspondence: Qin Chen, chen.qin@scu.edu.cn
#These authors contributed equally.

Abstract

Idiopathic normal pressure hydrocephalus (iNPH) is a clinical syndrome characterized by cognitive decline, gait disturbance, and urinary incontinence. As iNPH often occurs in elderly individuals prone to many types of comorbidity, a differential diagnosis with other neurodegenerative diseases is crucial, especially Alzheimer's disease (AD). A growing body of published work provides evidence of radiological methods, including multimodal magnetic resonance imaging and positron emission tomography, which may help noninvasively differentiate iNPH from AD or reveal concurrent AD pathology *in vivo*. Imaging methods detecting morphological changes, white matter microstructural changes, cerebrospinal fluid circulation, and molecular imaging have been widely applied in iNPH patients. Here, we review radiological biomarkers using different methods in evaluating iNPH pathophysiology and differentiating or detecting concomitant AD, to noninvasively predict the possible outcome postshunt and select candidates for shunt surgery.

Keywords: idiopathic normal pressure hydrocephalus; Alzheimer's disease; radiological biomarker; magnetic resonance imaging; positron emission tomography

Introduction

Idiopathic normal pressure hydrocephalus (iNPH) is a clinical syndrome characterized by cognitive decline, gait disturbance, and urinary incontinence (Adams *et al.*, 1965) with a prevalence of 0.2% in populations aged 70–79 years and 5.9% in 80 years and older (Jaraj *et al.*, 2014). Shunt surgery is an effective treatment for iNPH, while the cerebrospinal fluid tap test (CSFTT) is a common method to predict whether iNPH patients can benefit from further shunt surgery (Graff-Radford *et al.*, 2019), but the application of CSFTT was clinically confined due to its relatively low sensitivity and invasiveness (Thavarajasingam *et al.*, 2021). Therefore, radiological approaches may provide noninvasive biomarkers for identifying possible shunt responders (Craven *et al.*, 2016).

On the other hand, since iNPH often occurs in elderly individuals prone to many types of comorbidity, a differential diagnosis with other neurodegenerative diseases is crucial, especially with Alzheimer's disease (AD) (Malm *et al.*, 2013). Several studies based on brain biopsy have also supported that AD is a common pathologic comorbidity with iNPH, and distinguishing these patients may help in the selection of probable shunt responders (Cabral *et al.*, 2011; Pomeraniec *et al.*, 2016).

A growing body of reports provide evidence that multimodal magnetic resonance imaging (MRI), including structural MRI, diffusion tensor imaging, phase-contrast MRI, and glymphatic MRI, as well as positron emission tomography (PET) may help noninvasively differentiate iNPH from AD and discover concurrent AD pathology *in vivo* (Ishii *et al.*, 2008; Leinonen *et al.*, 2018; Park *et al.*, 2021). Therefore, this study set out to review the usefulness of various radiological biomarkers in the differential diagnosis of iNPH and AD and their value in the prediction of shunt responders in iNPH patients.

Structural MRI

Structural MRI (sMRI) is the most useful model in clinical practice due to its accessibility. Common morphological hallmarks of iNPH on sMRI include increased Evan's index (EI), sharpened callosal angle (CA), and disproportionately enlarged subarachnoid space (DESH) (Agerskov *et al.*, 2019) (Fig. 1). Extensive series of volumetric and voxel-based analysis (VBA) studies have quantitatively measured these changes (Ishii *et al.*, 2008; Moore *et al.*, 2012; Yamashita *et al.*, 2014).

EI was first proposed in 1942 as the ratio of the maximal width of the frontal horns of both lateral ventricles to the maximum inner skull diameter (Evans, 1942). It was recognized as an estimation of ventricular volume, with an EI > 0.3 defined as ventriculomegaly (Toma *et al.*, 2011). However, with progress in brain scan techniques, researchers have found that EI is related to age, sex, and scan plane (Toma *et al.*, 2011). A large population-based study demonstrated that EI ranged from 0.11 to 0.46 in individuals aged ≥70 years, and 20.6% of them had an EI > 0.3 (Jaraj *et al.*, 2017). Another study derived new cutoff values of EI based on age

Received: 16 September 2022; **Revised:** 18 November 2022; **Accepted:** 24 November 2022

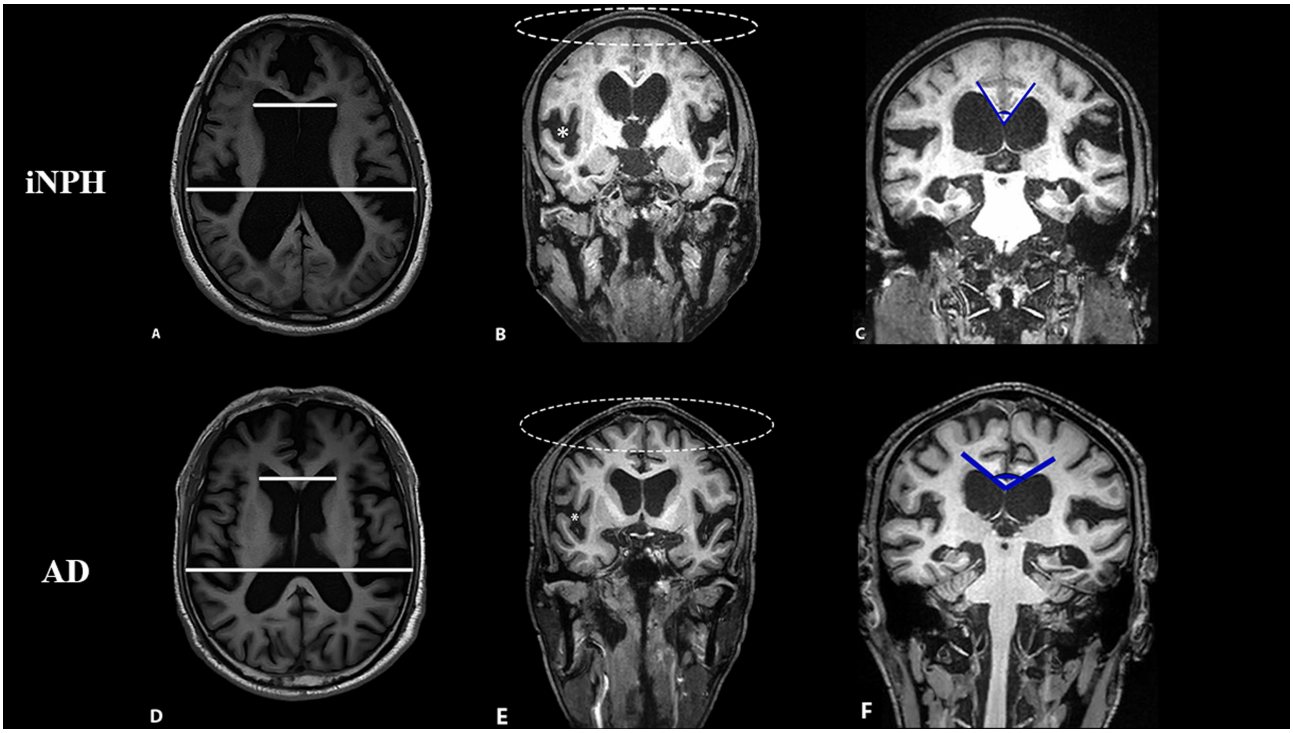

Figure 1: Common morphological hallmarks of iNPH. (A)–(C) were taken from an 80-year-old iNPH patient with a positive CSFTT, and (D)–(F) were taken from a 76-year-old AD patient. (A) and (D) demonstrate the measurement of EI. These two patients both had an EI > 0.3 (A, EI = 0.36: D, EI = 0.34); thus, EI seems unreliable for distinguishing iNPH and AD. (B) and (E) demonstrate that iNPH patients have a different CSF distribution from AD patients. CSF volume significantly increased in ventricles and Sylvian fissures but decreased in the superior convexity and medial subarachnoid spaces, termed DESH. (C) and (F) show the measurement of CA. CA should be measured on a coronal plane perpendicular to the AC–PC line on the posterior commissure plane, and 90° is a common cutoff value for differentiating iNPH from AD (C, CA = 69°; F, CA = 109°).

and sex from AD cohorts and healthy elderly controls, and further validated them in a small sample of probable iNPH patients. It finally showed a sensitivity of 80% for differentiating iNPH from controls using a revised cutoff value of EI (Brix *et al.*, 2017). As there is a major overlap of EI between iNPH and AD (also known as 'hydrocephalus *ex vacuo*'), using EI solely to exclude neurodegenerative diseases seems unreliable (Nakajima *et al.*, 2021) (Fig. 1A and D).

CA, another traditional radiological marker, was initially discovered using pneumoencephalography (Benson *et al.*, 1970). The renewed concept of CA based on computed tomography or MRI scans should be measured on a coronal plane perpendicular to the anterior commissure–posterior commissure (AC–PC) line on the posterior commissure plane (Ishii *et al.*, 2008). A recent meta-analysis evaluated the diagnostic performance of CA in iNPH patients with low heterogeneity. The pooled sensitivity was 91%, and the specificity was 93% when using CA to diagnose iNPH and five out of seven studies using a cutoff value of 90° (Park *et al.*, 2021). Unlike EI, CA could reflect specific iNPH pathogenesis, since a sharp CA often suggests an elevation due to the dilation of lateral ventricles and Sylvian fissures and thus assists the differential diagnosis of iNPH with AD (Ishii *et al.*, 2008). Several studies have revealed that using 90° as a cutoff value yielded a sensitivity of 84–97% and specificity of 64–95% when differentiating probable iNPH and AD (Ishii *et al.*, 2008; Kim *et al.*, 2021; Mantovani *et al.*, 2020) (Fig. 1C and F). As mentioned before, EI has little value in differentiating iNPH and AD, but when using EI and CA in combination, the differential diagnostic performance could be further improved compared to using CA alone (Ishii *et al.*, 2008; Miskin *et al.*, 2017).

Moreover, researchers have found that there is a different pattern of CSF distribution between iNPH and brain atrophy. Kitagaki *et al.* compared four main CSF compartments using coronal MR images in shunt-responsive iNPH and matched AD and vascular dementia patients (Kitagaki *et al.*, 1998). This study first reported a different CSF distribution pattern between iNPH and AD, with the CSF volume significantly increased in ventricles and Sylvian fissures but decreased in the superior convexity and medial subarachnoid spaces (Kitagaki *et al.*, 1998). Then, a multicenter cohort study validated the diagnostic value of these signs and termed them DESH (Hashimoto *et al.*, 2010) (Fig. 1B and E). Studies have elucidated that DESH exhibits the ability to distinguish shunt responders and nonresponders (Craven *et al.*, 2016; Hashimoto *et al.*, 2010; Narita *et al.*, 2016; Virhammar *et al.*, 2014). The estimated positive predictive value of DESH for shunt responders was 77% but with a relatively low negative predictive value of only 25% (Craven *et al.*, 2016). While these findings suggest DESH is a great diagnostic tool for iNPH and reflects the prognosis to some extent, it is still not sufficient to replace CSFTT.

Several different methods have made these morphological changes quantitative, with volumetric analysis and VBM being the most common methods. Quantitative measurements of ventricular volume and total cortical thickness in combination can improve iNPH differential diagnosis with AD (Moore *et al.*, 2012). VBA demonstrated that increased gray matter density of para-interhemispheric gyri and frontoparietal cortices at high convexity can be used as important markers for differentiating iNPH and AD, since it underlies the pathophysiology of iNPH such as DESH (Ishii *et al.*, 2008). Although hippocampal volume is considered a biomarker of neurodegeneration in AD, iNPH patients

also demonstrated alterations in hippocampal volume. It was first reported that iNPH patients exhibited a minor left-side decrease in hippocampal volumes, and this different pattern may provide diagnostic discrimination from AD (Savolainen *et al.*, 2000). The voxel-based morphometry study, however, confirmed bilateral hippocampal volume loss in iNPH patients, while it was relatively retained compared to AD (Ishii *et al.*, 2008). Whether AD pathology complicates the diagnosis of iNPH in this study is unknown (Golomb *et al.*, 1994). Voxel-based morphometry of CSF space was also conducted on shunt-responsive iNPH and AD patients, with ventricular/sylvian and high convexity/midline (HCM) being used as regions of interest (Yamashita *et al.*, 2014; Yamashita *et al.*, 2010). The results indicated that the ratio of these two regions of interest (ventricular/sylvian/HCM) was significantly higher than that of AD, exhibiting a sensitivity of 89% and specificity of 100% for differential diagnosis (Yamashita *et al.*, 2014). In addition, this ratio was related to the improvement of gait and cognitive function after shunting, supporting the idea that milder brain deformation could have larger improvements after shunt surgery (Yamamoto *et al.*, 2013).

Recent studies still attach great importance to these traditional markers, and several newly proposed imaging biomarkers were derived from these traditional ones. Inspired by EI and DESH, Yamada *et al.* found that z-axial expansion of lateral ventricles and compression at convexity may be common parameters for differential diagnosis and further established the z-axial EI (z-EI) and brain-to-ventricle ratios: two new radiological markers to differentiate iNPH from AD (Yamada *et al.*, 2016; Yamada *et al.*, 2015). As CA has already been validated in several studies, researchers seek to measure CA at the anterior commissure level, called the anterior CA (ACA), which clearly differentiates iNPH from AD with a sensitivity of 93% and specificity of 83% (Mantovani *et al.*, 2021). Further investigations are needed to validate these findings in larger populations.

To date, structural MRI is still the most useful method for the clinical evaluation of iNPH, considering its overall accessibility, and could be interpreted visually. Traditional radiological markers reflected by sMRI still reveal a good performance of differential diagnosis and prognostic prediction, while their absence should not exclude iNPH patients from shunt surgery (Agerskov *et al.*, 2019; Chen *et al.*, 2022; Ishii *et al.*, 2008; Virhammar *et al.*, 2014). More importantly, these radiological changes were confirmed to precede the onset of iNPH symptoms or only with subclinical cognitive decline (Engel *et al.*, 2018; Engel *et al.*, 2021) and thus may become a preferable screening tool for preclinical iNPH patients in the future.

Diffusion tensor imaging

Diffusion tensor imaging (DTI) is a rapidly developing noninvasive MRI-based imaging technique that was proposed in 1994 (Basser *et al.*, 1994a; Basser *et al.*, 1994b), which can detect microstructural integrity and orientation of white matter by measuring the intracranial directionality and scale of water diffusion (Beaulieu, 2009; Winston, 2012). There are many tensor-derived quantitative parameters commonly used in DTI-based analysis of microstructural WM integrity, including axial diffusivity (reflecting the parallel diffusion of the axon), radial diffusivity (reflecting the perpendicular diffusion of the axon) (Klawiter *et al.*, 2011), mean diffusivity [MD, meaning the mean motion of water (Rose *et al.*, 2008)], and fractional anisotropy (FA, commonly used for measuring diffusion anisotropy of the water (Teipel *et al.*, 2016)).

In recent years, DTI has been regarded as one of the most sensitive and promising imaging biomarkers for the diagnosis of iNPH due to its excellent ability to reflect changes in white matter microstructure, and many studies have found that iNPH has unique DTI alterations compared with healthy controls and other neurodegenerative diseases (such as AD) because of its unique pathophysiological mechanism (Caligiuri *et al.*, 2022; Daouk *et al.*, 2014; Grazzini *et al.*, 2021; Hattori *et al.*, 2011; Hong *et al.*, 2010; Horinek *et al.*, 2016; Hoza *et al.*, 2015; Ivkovic *et al.*, 2013; Kang *et al.*, 2016; Kanno *et al.*, 2011; Kanno *et al.*, 2017; Koyama *et al.*, 2013; Scheel *et al.*, 2012; Siasios *et al.*, 2016; Younes *et al.*, 2019) (Table 1). Most studies indicate that iNPH has widespread diffusion changes in the corpus callosum (CC) and periventricular white matter (Caligiuri *et al.*, 2022; Hattori *et al.*, 2011; Hong *et al.*, 2010; Horinek *et al.*, 2016; Kang *et al.*, 2016; Kanno *et al.*, 2011; Koyama *et al.*, 2013; Younes *et al.*, 2019). Significantly lower mean hemispheric FA and higher mean hemispheric MD have been found in iNPH patients than AD and PD patients, and VBA showed that iNPH patients have significantly higher MD values in the CC and periventricular white matter and have significantly lower FA values in the CC (Kanno *et al.*, 2011). Similar FA and MD changes in the CC were also found in studies using tract-based spatial statistics (TBSS) than in healthy controls and AD patients (Kang *et al.*, 2016; Koyama *et al.*, 2013). Moreover, iNPH patients have more altered principal diffusion direction (V1) voxels in the midsagittal portion of the splenium along the CC, which is significantly different from AD patients (Bonferroni-corrected P value < 0.01) and has better diagnostic efficiency based on a random forest classifier than other diffusivity parameters [$AUC_{iNPH\ vs.\ AD} = 0.88$ (95% CI: 0.76–1)] (Caligiuri *et al.*, 2022). Additionally, many studies have shown that patients with iNPH also have significant diffusivity parameter changes compared with AD patents in paraventricular white matter fibers, such as the anterior corona radiata [including corticomedullary tract, corticospinal tract (CST), thalamic radiation, and thalamic, etc.] and thalamic radiation, which indicate impaired white matter integrity (Hattori *et al.*, 2011; Hong *et al.*, 2010; Horinek *et al.*, 2016; Kang *et al.*, 2016; Koyama *et al.*, 2013; Younes *et al.*, 2019). INPH patients present significantly lower FA in the anterior corona radiata and superior longitudinal fasciculus based on TBSS. Decreased FA was also found in cortico-pontocerebellar pathway fibers (i.e. bilateral posterior thalamic radiation, external capsules, and middle cerebellar peduncles), which awaits further study (Kang *et al.*, 2016; Schmahmann *et al.*, 2006). The decreased FA and increased MD in the CC and periventricular white matter in the iNPH patients discussed before may be caused by axonal degeneration and interstitial edema based on the mechanical pressure of dilated ventricles (Mataró *et al.*, 2007; Medina *et al.*, 2008; Röricht *et al.*, 1998; Uluğ *et al.*, 2003).

In addition, most studies have demonstrated that iNPH patients have higher FA values in the white matter of the paraventricular tracts, especially the CST (Hattori *et al.*, 2011; Horinek *et al.*, 2016; Younes *et al.*, 2019). A study focusing on CST fibers in iNPH patients found significantly increased FA values and axial diffusivity in the CST of iNPH patients based on tract-specific analysis. They also showed that CST fibers of iNPH patients have higher anisotropy and are straighter than patients with AD in visual evaluation of tractography (Hattori *et al.*, 2011). Similarly, iNPH patients also have increased FA, MD, and axial diffusivity in the corticoefferent tracts adjacent to the lateral ventricles, which correlated with ventricular volumes (Horinek *et al.*, 2016). Positive correlation between ventricular volumes and the axial diffusivity was also found in the CST, which does not exist in AD patients. Interestingly, a similar correlation was also found in

Table 1: Methodology and results of included studies using DTI.

First author, year	Population	MR field strength	Voxel size (mm)	B values (s/mm^2)	Gradient directions	Analytical methodology	Study design	Key findings
Caligiuri ME, 2022	NPH 23 PSP 27 AD 35 HC 36	3T	2 × 2 × 2	1000	27	VBA	Cross-sectional	NPH patients have more altered principal diffusion direction (V1) voxels in the midsagittal portion of the splenium along the CC (significantly different from AD patients)
Younes K, 2019	NPH 9 AD 13 HC 20	3T	2 × 2 × 2	1000	64	TPA	Cross-sectional	NPH patients presents a positive correlation between ventricular volumes and the axial diffusivity of CST, which was also found in superior thalamic radiation
Kanno S, 2017	SR 28 SNR 8 HC 10	1.5T	2.5 × 2.5 × 2.5	1000	13	TBSS	Longitudinal	FA value in the corona radiata decreased after shunt surgery that only happened in the SR group
Kang K, 2016	NPH 28 AD 28 HC 20	3T	2 × 2 × 2	600	45	TBSS, RBA	Cross-sectional	NPH patients exhibited lower FA and higher MD in bilateral anterior corona radiata, superior longitudinal fasciculus, and cortico-ponto-cerebellar pathways than AD patients
Hořínek D, 2016	NPH 17 AD 14 HC 17	3T	1.8 × 1.8 × 2.4	1000	30	TBSS	Cross-sectional	NPH patients showed higher FA, MD, and axial diffusivity in the cortico-fugal tracts that is correlated with ventricular volumes (significantly different from AD patients)
Daouk J, 2014	NPH 12 AD 18	3T	3 × 3 × 3	1000	12	RBA	Cross-sectional	Aqueductal CSF stroke volume of NPH patient is NOT correlated with the axial diffusivity and radial diffusivity in the internal capsue (significantly different from AD patients)
Koyama T, 2013	NPH 24 HC 21	3T	1.8 × 1.8 × 3	1000	12	TBSS, RBA	Cross-sectional	NPH patients present significant lower FA in the CC and higher FA in the posterior limb of internal capsule

Table 1: Continued

First author, year	Population	MR field strength	Voxel size (mm)	B values (s/mm^2)	Gradient directions	Analytical methodology	Study design	Key findings
Ivkovic M, 2013	NPH 15 AD 9 PD/DLB 16	3T	1.8 × 1.8 × 2.5	1000	33	MD Histogram Analysis	Cross-sectional	The diagnostic model of MD Histogram Fitting based on Generalized Voss-Dyke fitting reached 86% sensitivity and 88% specificity in the NPH-AD task
Scheel M, 2012	NPH 13	1.5T	4 × 4 × 4	1000	25	TBSS	Longitudinal	The FA, MD, parallel diffusivity, and radial diffusivity tended to be normal after shunt surgery, although there were still significant differences from HC
Kanno S, 2011	NPH 20 AD 20 PD 20	1.5T	2.5 × 2.5 × 2.5	1000	13	VBA	Cross-sectional	NPH patients have significantly lower mean hemispheric FA and higher mean hemispheric MD compared with patients in AD and PD groups, and have significantly higher MD and lower FA value in the CC
Hattori T, 2011	NPH 18 AD 11 PDD 11 HC 19	1.5T	3 × 3 × 3	1000	13	TPA	Cross-sectional	NPH patients showed higher FA value and axial diffusivity in CST. In addition, NPH patients' CST fibers also have higher anisotropy and straighter than patients with AD in visual evaluation of tractography
Hong YJ, 2010	NPH 13 AD 15 HC 15	1.5T	4 × 4 × 4	1000	25	RBA	Cross-sectional	The FA value in hippocampal region is sorted from the highest to the lowest in HC-NPH-AD order, while the MD value in hippocampal region is sorted from the highest to the lowest in AD-NPH-HC order

Note: NPH, normal pressure hydrocephalus; HC, healthy control; SNR, shunt-nonresponsive NPH; PD, Parkinson's disease; PDD, Parkinson's disease dementia; DLB, dementia with Lewy bodies; TPA, tract-specific analysis; TBSS, tract-based spatial statistics; RBA, manual-region of interest-based analysis.

superior thalamic radiation (the most medial part of the superior corona), which uncovers further research and diagnostic value of correlations between macrostructural characteristics of ventricular and microstructural changes of paraventricular tracts (Younes *et al.*, 2019). INPH patients also have significantly higher FA in the posterior limb of the internal capsule where the CST is located (Koyama *et al.*, 2013). The widely identified paraventricular tract's increased FA and axial diffusivity in paraventricular tracts may be explained by fewer crossed fibers within the voxel due to the pressure-related stretching of the ventricles and compression of white matter fibers, which remains controversial (Grazzini *et al.*, 2021; Horinek *et al.*, 2016; Kim *et al.*, 2011).

Furthermore, several studies are expected to further explore the pathophysiological mechanisms of iNPH and complete its differential diagnosis with AD using DTI-based methods (Daouk *et al.*, 2014; Hong *et al.*, 2010; Ivkovic *et al.*, 2013). The FA value in the hippocampal region was found sorted from the highest to the lowest in the HC-NPH-AD order, while the MD value in the hippocampal region was sorted from the highest to the lowest in the AD-NPH-HC order using a region of interest-based method, which indicates different pathophysiological changes between AD and NPH patients; that is, the damage to hippocampal white matter microstructure due to mechanical pressure of CSF in iNPH patients is not as severe as the primary damage to hippocampal structure caused by AD (Hong *et al.*, 2010). Some studies have also proposed innovative biomarkers for classification. A classification model based on DTI histograms and the Voss-Dyke fitting method was proposed and obtained 86% sensitivity and 88% specificity in the iNPH-AD classification task (Ivkovic *et al.*, 2013). The relationship between CSF flow and diffusivity parameters can also be used for classification, the axial diffusivity and radial diffusivity in the internal capsule of AD patients are correlated with the aqueductal CSF stroke volume, while there is no similar correlation in patients with iNPH, which may be due to the forced diffusion of CSF in AD patients and needs to be studied further (Daouk *et al.*, 2014).

The pathogenesis of iNPH is still unclear, and it is generally believed that it is related to the universal damage of the periventricular white matter due to ventricular dilation and abnormal CSF dynamics (Jurcoane *et al.*, 2014; Skalický *et al.*, 2020; Wang *et al.*, 2020). At the initial stage of iNPH, various factors led to the increase in CSF pulsatility (Hayashi *et al.*, 2015; Wagshul *et al.*, 2011) and made hyperdynamic CSF flow more to the ventricles (Ringstad *et al.*, 2016), which increased the shearing forces and compressive stress (Capone *et al.*, 2020; Jacobsson *et al.*, 2018) on the inner wall of the ventricles, causing ventricular expansion. At the same time, the decrease in CSF drainage caused by factors such as decreased intracranial compliance and increased venous pressure will also promote this process (Jacobsson *et al.*, 2018). Ventricular dilation will increase pressure on a larger surface area and further reduce CSF drainage, leading to a vicious cycle (Greitz *et al.*, 1994; Rekate *et al.*, 2008). Expansion of the ventricles with their increased mechanical stress on the surface can cause compression and deformation of the periventricular white matter, which in turn leads to the main clinical symptoms of iNPH (e.g. CST compression causing gait disturbance and urinary incontinence) (Holodny *et al.*, 2005; Relkin *et al.*, 2005). These DTI-based method studies all showed that iNPH patients have higher FA values in the white matter of the paraventricular tracts, which indicates that axons are densely packed in paraventricular tracts (Horinek *et al.*, 2016; Hattori *et al.*, 2011; Horinek *et al.*, 2016). The increase in FA was found limited to the region near the lateral ventricle of the CST, confirming the previous "compression hypothesis" (Hattori *et al.*, 2011). According to the clinical guidelines, shunt surgery is the recommended therapy for early iNPH patients, which can largely modify abnormal CSF dynamics, reduce mechanical stress and white matter compression on the ventricular wall, and then relieve clinical symptoms (Mori *et al.*, 2012). Some studies using the DTI-based method confirmed the previously mentioned changes in white matter microstructure (Kanno *et al.*, 2017; Scheel *et al.*, 2012). The FA, MD, parallel diffusivity, and radial diffusivity tended to be normal after shunt surgery, although there were still significant differences from healthy controls, which indicated a recovery of reversible damage caused by white matter compression (Scheel *et al.*, 2012). Moreover, the closer the paraventricular tract is to the ventricle, the greater the preoperative FA value increases, and the greater the postoperative FA value decreases, indicating that the closer the paraventricular tract is to the ventricle, the more obvious the compression is. Meanwhile, the relative changes in FA and axial diffusivity before and after shunt surgery can be used as a good tool to predict shunt response, indicating that the recovery of paraventricular tract compression after surgery is positively correlated with the improvement of symptoms (Jang et al., 2011). There are also studies devoted to the prognosis prediction of iNPH patients after shunt surgery and trying to determine the potential reasons for poor shunt response. Compared with shunt-responsive (SR) patients, the volume of the cerebral ventricle in nonresponsive NPH (NR) decreased slightly after the operation, indicating that the decrease in insufficient pressure adjustments or ventricular compliance is a possible cause of NR. Additionally, compared with SR, MD in the left hemisphere of NR increased after shunt surgery, which may represent the expansion of interstitial edema and irreversible damage of white matter microstructure (Kanno *et al.*, 2017). Interestingly, in some NRs, although the axial diffusivity of the CST was significantly reduced after surgery (representing a decrease in mechanical stress in the ventricular wall), their clinical symptoms were not significantly relieved, which also indicated that NR caused irreversible damage to periventricular white matter (Jurcoane *et al.*, 2014). Neuropathological studies have confirmed that, in addition to the axons themselves packed, the mechanical stress of ventricular expansion may also lead to decreased blood flow perfusion (Takeuchi *et al.*, 2007), metabolic abnormalities (especially the abnormal glymphatic system) (Tan *et al.*, 2021), and neuroinflammation (Zhou *et al.*, 2019) in the peripheral white matter and further cause irreversible axonal damage, which can also explain the increase in axial damage biomarkers in the CSF of some patients with iNPH (such as neurofilament light protein) (Jeppsson *et al.*, 2013). DTI-based methods can be used to find compression and irreversible damage to the paraventricular tract through diffusion changes before and after shunt surgery and can be used as promising noninvasive biomarkers to distinguish SR and NR.

In general, DTI-based methods can detect changes in white matter microstructure (especially CC and periventricular white matter) in patients with iNPH before structural MRI. On this basis, we can study the unique pathophysiological changes of iNPH, which can be used for differential diagnosis with other neurodegenerative diseases (such as AD). Meanwhile, the DTI-based method can also analyze the changes in white matter microstructure before and after shunt surgery in patients with iNPH and serve as a promising, noninvasive diagnostic and prognostic evaluation method for iNPH. However, there are still some remaining limitations requiring further DTI-based research for iNPH, such as interpretation of conflicting results, significant inter-scanner differences and difficulties in processing data of crossing white matter tracts (Alexander *et al.*, 2001; Lenfeldt *et al.*, 2011; Moura *et al.*, 2019).

Phase-contrast MRI (PC-MRI)

MRI was thought to be an effective tool for the detection of CSF flow. It was first reported that iNPH exhibited hyperdynamic CSF motion and decreased ventricular compliance and therefore presented with significant aqueductal signal loss in MR images compared to brain atrophy, termed the "CSF flow void sign" (Bradley *et al.*, 1986). However, previous studies have found that it has little predictive value for shunt responders in patients with iNPH (Bradley *et al.*, 1996; Krauss *et al.*, 1997). Therefore, a new method of quantitatively measuring CSF flow by MRI was proposed and extensively applied in iNPH research, that is, PC-MRI (Edelman *et al.*, 1986). PC-MRI is the only MRI technique to visualize CSF motion thus far, and most of the clinical CSF flow measurements have been carried out in the aqueduct (Connor *et al.*, 2001). Since its early application in iNPH, multiple studies have sought to answer the question of "how to distinguish shunt responders from nonresponders" through this technique. Aqueductal stroke volume (SV) was defined as the total amount of CSF pulsating caudally (or cranially) through the aqueduct in one cardiac cycle, with a normal range of 30–50 μl across studies, while iNPH is characterized by significantly increased SV (Greitz *et al.*, 1994; Wagshul *et al.*, 2006; Yamada *et al.*, 2015). Bradley *et al.* first reported a threshold of 42 μl in differentiating shunt responders from nonresponders, with a sensitivity of 80% and specificity of 100% (Bradley *et al.*, 1996). They supposed that this increase in SV may contribute to the squeezing of dilated ventricles, while a continuous pressure gradient further led to the collapse of periventricular arterioles and progressive ischemia, causing irreversible diminished pump function and then decreased SV (Bradley *et al.*, 1996; Scollato *et al.*, 2008). Another study also showed that a CSF flow rate of >18 ml/min could distinguish iNPH from other forms of cognitive impairment (Luetmer *et al.*, 2002). Other researchers, however, have found limited significance when using PC-MRI to predict shunt outcome (Dixon *et al.*, 2002; Kahlon *et al.*, 2007). These contradictory results suggest a difficulty in exclusion of AD hydrodynamics comorbid with iNPH (Bateman *et al.*, 2007; Takizawa *et al.*, 2017) and, moreover, an urgent need in protocol standardization with the PC-MRI method. The selection of proper sequence parameters such as velocity encoding is essential for the high quality of PC-MR images and their clinical application when using quantitative measurements (Korbecki *et al.*, 2019). Therefore, Bradley *et al.* highlighted that medical centers should establish their own aqueductal SV cutoff value, which is twice as high as that derived from healthy volunteers (Bradley, 2015). For these reasons, quantitative PC-MRI studies may exhibit huge inconsistency, while they still hold promise for differential diagnosis and prognostic prediction for iNPH in an experienced single center.

Glymphatic MRI

In addition to the aforementioned hydrodynamic changes, iNPH patients also have disturbed CSF homeostasis. Iliff *et al.* first reported that there is a kind of system in rodents, where CSF flows into the brain parenchyma from the periarterial space and flows out from the perivenous space after material exchange with the interstitial fluid (Iliff *et al.*, 2012). This system was termed as the "glymphatic system," as it has a structure and function similar to those of the lymphatic system, and aquaporin 4 (AQP4) is the main protein that mediates this material exchange. This system is believed to be involved in the clearance of β-amyloid, one of the pathological hallmarks of AD (Iliff *et al.*, 2012; Shokri-Kojori *et al.*, 2018), and the pathogenesis of many neurological diseases (Rasmussen *et al.*, 2018).

Following intrathecal injection of a paramagnetic contrast agent, CSF-ISF exchange across the rat brain was seen using the dynamic contrast-enhanced MRI method for the first time (Iliff *et al.*, 2013). The perfusion of the glymphatic system was also measured by MRI method in stroke mouse models, which demonstrated significant impairment of glymphatic system perfusion after subarachnoid hemorrhage and acute ischemic stroke (Gaberel *et al.*, 2014). Glymphatic MRI was first applied in iNPH patients and controls in 2017 by intrathecally injected gadobutrol as an MR contrast agent, to assess brain glymphatic function (Ringstad *et al.*, 2017). Delayed enhancement and reduced clearance of gadobutrol at the Sylvian fissure was observed in iNPH patients. They further interpreted as signs of reduced glymphatic clearance in iNPH patients (Ringstad *et al.*, 2017). Another study with longer MR scan time points also demonstrated similar impairments in glymphatic flux (Ringstad *et al.*, 2018). A more recent survey revealed that delayed clearance of gadobutrol also occurred in the entorhinal cortex and adjacent white matter, which is pivotal for cognitive function (Eide *et al.*, 2019). Hence, it could be conceivably hypothesized that reduced glymphatic clearance may be attributed to waste accumulation, such as β-amyloid, in these cognitive brain networks and then induce dementia or comorbidities, such as AD. Further investigations should be focused on the clinical value of glymphatic MRI to recognize patients with concurrent AD and whether there is any association between shunt implantation and CSF clearance.

Altogether, these MRI methods for evaluating CSF circulation may contribute to our knowledge of the underlying mechanism of iNPH pathogenesis but with little evidence of clinical application thus far. Further studies are required to determine a set of standardized protocols for these MRI methods and then testify to the consistency across studies.

Positron emission tomography

PET is currently one of the most popular methods for investigating neurodegenerative diseases, especially in the AD research field. Several PET modalities have already been established in iNPH for differential diagnosis and prognostic prediction.

In terms of the detection of metabolic changes in iNPH patients, Jagust *et al.* first used ^{18}F-fluorodeoxyglucose (FDG)-PET to demonstrate a different pattern of metabolic abnormalities between iNPH and AD in 1985. The brains of patients with AD showed bilateral temporoparietal hypometabolism, while those of patients with iNPH demonstrated global metabolic changes in iNPH (Jagust *et al.*, 1985). Another study in 1995 also demonstrated similar metabolic changes in iNPH (Tedeschi *et al.*, 1995). A recent retrospective study compared the pattern of FDG-PET between iNPH and several neurodegenerative diseases (including AD) using VBA. The authors found that AD exhibited cortical hypometabolism, while iNPH had a pattern of subcortical hypometabolism, including bilateral dorsal striatum, even after partial volume correction (Townley *et al.*, 2018). Differences between these studies may arise from the improved partial volume correction and patient selection. Several studies also sought to investigate metabolic changes before and after shunt surgery. Patients with iNPH underwent clinical assessment and FDG-PET before and 1 week after a shunt procedure. These two studies yielded similar results that the cerebral metabolic rate of glucose (CMRglu) significantly increased among shunt responders, and there was a correlation between metabolic change and clinical symptoms (Calcagni *et al.*, 2012;

Calcagni *et al.*, 2013). Therefore, FDG-PET serves as an excellent tool to differentiate iNPH and other neurodegenerative diseases and as a biomarker of response to intervention, although it cannot define whether an iNPH patient responds to shunt surgery.

The accumulation of β-amyloid (Aβ) and phosphorylated Tau protein are considered pathological hallmarks of AD. While an autopsy study confirmed that AD is a common pathologic comorbidity in iNPH patients and may preclude improvement after shunt surgery (Cabral *et al.*, 2011), it is necessary to develop a noninvasive method to detect AD pathology in the setting of iNPH. Thanks to the major improvement of CSF biomarkers and molecular imaging techniques, *in vivo* detection of AD pathology has become realized and increasingly applied in the iNPH research field in the last few decades (Table 2). Common Aβ tracers, including ^{11}C-Pittsburgh compound-B (PiB), ^{18}F-Flutemetamol, ^{18}F-Florbetaben (FBB), and ^{11}C-BF227, were adopted in iNPH patients to detect amyloid pathology (Hiraoka *et al.*, 2015; Jang *et al.*, 2018; Leinonen *et al.*, 2008; Rinne *et al.*, 2012). ^{11}C-PiB PET and frontal cortical brain biopsy were first appied to evaluate Aβ load. A total of four out of seven iNPH patients have a biopsy-confirmed Aβ and increased PiB uptake (Leinonen *et al.*, 2008), while the PiB distribution pattern was different from AD, since PiB retention was limited to the high-convexity parasagittal areas in iNPH patients (Jiménez-Bonilla *et al.*, 2018; Kondo *et al.*, 2013). Several studies using ^{18}F-Flutemetamol and brain biopsy also demonstrated similar Aβ deposition in iNPH patients, and confirmed the concordance of Aβ-PET imaging with histopathology (Leinonen *et al.*, 2013; Rinne *et al.*, 2012; Wolk *et al.*, 2011; Wong *et al.*, 2013). Longitudinal studies were carried out to evaluate Aβ deposition with clinical improvement after shunt surgery. A recent study found a significant correlation between neocortical ^{11}C-BF227 SUVR and cognitive improvement reflected by the iNPH grading scale after shunt surgery (Hiraoka *et al.*, 2015). Other studies using Flutemetamol or Florbetaben have also indicated that Aβ+iNPH patients have a higher frequency of CSFTT responder and shunt responsiveness, as they may be more likely to experience a secondary deterioration after surgery (Jang *et al.*, 2018; Jang *et al.*, 2022). Overall, these results suggest that Aβ pathology tested by PET was consistent with CSF or histopathology findings and that discriminating concurrent AD pathology may help in the selection of probable shunt candidates with iNPH. However, the long-term prognostic value of Aβ-PET in postshunt iNPH patients remains to be elucidated.

In addition, Aβ-PET may be an effective tool in the search for iNPH pathogenesis. A recent meta-analysis was conducted to clarify the Aβ biomarkers in the CSF of iNPH patients, which illustrated a significantly decreased level of CSF Aβ42 compared to normal controls but a slight increase compared to AD patients (Chen *et al.*, 2017). Researchers have put forward different opinions for Aβ level reductions in CSF. Dr. Graff-Radford hypothesized that the glymphatic pathway was impaired in the setting of iNPH, leading to decreased clearance of Aβ and its precursors (Graff-Radford, 2014). Another researcher explained it in terms of periventricular hypometabolism seen on FDG-PET or MRI (Jeppsson *et al.*, 2013). However, a study found that two iNPH patients with higher cortical PiB retention had the lowest level of CSF Aβ42, thus supporting the actual Aβ deposition in the cerebral cortex of iNPH patients (Kondo *et al.*, 2013). Large-scale studies are still needed to clarify the underlying pathogenesis of altered Aβ biomarkers in iNPH patients.

Notably, it was reported that Aβ deposition reflected by Aβ-PET SUVR may be 15–20 years before cognitive symptom onset (Fleisher *et al.*, 2012). Aβ deposition was proven to reach a plateau; thus, another pathological protein may mediate cognitive impairment in the AD continuum (Jack *et al.*, 2013). An accumulating body of evidence has indicated the interaction between Aβ and Tau, in which they seem to be both the trigger and the bullet in AD pathogenesis (Bloom, 2014). Several studies suggest that Tau-PET is a promising tool for predicting cognitive change and is superior to Aβ-PET and MRI (Bischof *et al.*, 2017; Ossenkoppele *et al.*, 2021). One study explored both Aβ and Tau through biopsy, CSF analysis and PET imaging. Brain biopsy has confirmed that Tau accumulation also occurs in iNPH patients (3/14), although it is relatively rare compared to Aβ (9/14) (Leinonen *et al.*, 2018). However, further investigation used S-^{18}F-THK-5117 as a Tau-PET tracer but failed to demonstrate a significant correlation between S-^{18}F-THK-5117 uptake and biopsy-confirmed or CSF phosphorylated Tau (Leinonen *et al.*, 2018). This result may be explained by the off-target binding or small sample size of this study; thus, further research is needed to evaluate different Tau-PET tracers in larger-scale iNPH patient cohorts.

Limitations

Although previous studies have successfully demonstrated that radiological methods are becoming a promising tool in evaluating the prognosis for iNPH patients, a number of limitations need to be noted (Fig. 2). The principal limitation is the variable definition of shunt responder. In a recent multicenter randomized trial SINPHONI-2, researchers defined a favorable outcome as an improvement of one or more on the modified Rankin scale (mRS) at 3 months after randomization (Kazui *et al.*, 2015). However, several studies have also applied the improvement of MMSE, walking tests or even subjective reports of improvement (El Ahmadieh *et al.*, 2019; Kang *et al.*, 2016). The lack of a standardized evaluation method for shunt responders may result in inconsistencies across studies. Thus, a multidisciplinary team including a neurosurgeon, behavioral neurologist, psychiatrist, urologist, and physical therapist is highly recommended for comprehensively evaluating iNPH patients before and postshunt. Second, imaging techniques and postprocessing methods for DTI and PC-MRI need to be further standardized before clinical application. Third, the sample sizes of previous studies were relatively small, and the follow-up periods were limited. The generalizability of these findings and the long-term effects of shunt surgery still need to be validated in large-scale cohort studies in the future.

Conclusion

Taken together, previous investigations have suggested that iNPH is a common disease in elderly patients and is prone to concomitant AD. This review concluded that novel radiological biomarkers using different methods were effective in evaluating iNPH pathophysiology and differentiating or detecting concomitant AD, therefore noninvasively predicting the possible outcome postshunt and helping select candidates for shunt surgery. Although these findings should be interpreted with caution, no single method could rule out possible shunt responders thus far. Therefore, multidisciplinary methods and comprehensive evaluation of clinical symptoms pre- and post-CSFTT and radiological biomarkers seem to be the most effective protocols. Since the contribution of concomitant AD to the long-term outcome of iNPH patients remains elusive, large randomized controlled trials could provide more definitive evidence in the future.

Table 2: PET studies for evaluating concomitant AD pathology in patients with iNPH.

First author, year	Patient number	Study design	Tracers	Evaluating methods	Key findings
Leinonen, 2008	7	Cross-sectional	^{11}C-PiB	PET + frontal biopsy	4/7 have biopsy confirmed Aβ plaques and increased PiB uptake.
Wolk, 2011	7	Cross-sectional	^{18}F-Flutemetamol	PET + frontal biopsy	4/7 have biopsy confirmed Aβ plaques and positive PET scans. 3/7 negative flutemetamol scans were all in patients without evidence of Aβ plaque pathology.
Rinne, 2012	52	Pooled analysis of 2 prospective ($n = 30$) and 2 retrospective ($n = 22$) studies	^{18}F-Flutemetamol	PET + frontal or parietal biopsy	3/52 with inapplicable data. 14/52 were classified as abnormal for fibrillar Aβ based on biopsy. 13/52 were classified as abnormal for Aβ-PET.
Wong, 2013	12	Prospective	^{18}F-Flutemetamol	PET + parietal biopsy	2/12 with insufficient amount of tissue in the biopsy sample. 2/12 were classified as abnormal for fibrillar Aβ based on both overall biopsy and Aβ-PET. 8/12 were classified as normal based on both overall biopsy and Aβ-PET.
Leinonen, 2013	15	Prospective	^{11}C-PiB ($n = 7$) and ^{18}F-Flutemetamol ($n = 15$)	PET + frontal biopsy	4/15 suspected iNPH patients were classified as amyloid-positive based on overall pathology and all PET images were rated the same as the overall pathology read. ^{11}C-PiB PET imaging quantitative findings were concordant with ^{18}F-Flutemetamol.
Kondo, 2013	10	Cross-sectional	^{11}C-PiB	PET + CSF analysis	3/10 patients with iNPH without any clinical signs of AD had obvious cortical PiB retention, which is limited to the high-convexity parasagittal areas. High cortical PiB retention showed lower levels of CSF Aβ42, indicating the actual Aβ deposition rather than delayed CSF clearance.
Rinne, 2014	17	Prospective	^{18}F-Flutemetamol	PET + frontal biopsy	4/17 NPH patients were classified as amyloid-positive by overall pathology read. 3/17 were classified as positive for visual interpretation of Aβ-PET. In 4 biopsy amyloid-positive patients, the overall response was graded as good in 1, fair in 1, and transient in 2.
Hiraoka, 2015	10 iNPH + 10 AD + 10 HC	Prospective	^{11}C-BF227	PET only	5 patients with iNPH had neocortical SUVRs as high as AD patients. 5 patients with iNPH had neocortical SUVRs as low as HC. A significant correlation between neocortical SUVR and cognitive improvement after shunt surgery was observed.

Table 2: Continued

First author, year	Patient number	Study design	Tracers	Evaluating methods	Key findings
Jime´nez-Bonilla, 2018	13	Cross-sectional	^{11}C-PiB	PET only	3/13 iNPH patients showed a very high intense PiB retention in all of the cortical regions. 7/13 showed cortical PiB retention equal or more intense than controls, mainly in the upper parasagittal areas. 3/13 did not show any cortical retention higher than controls.
Jang, 2018	31	Prospective	^{18}F-Florbetaben	PET + CSF analysis	7/31 possible iNPH patients were classified as iNPH/FBB+ group, other 24/31 patients were classified as iNPH/FBB− group. Higher frequency of CSFTT responders in the iNPH/FBB− (83.3%) group compared to the iNPH/FBB+ group (28.6%). The iNPH/FBB+ group had significantly lower CSF Aβ42 and higher t-tau levels than iNPH/FBB− group. Patients with positive AD biomarkers are expected to be less responsive to shunt surgery.
Kang, 2018	17	Prospective	^{18}F-Florbetaben	PET only	iNPH patients showed remarkably higher FBB retention in bilateral frontal, parietal and occipital areas compared to HC. FBB retention in right frontal cortex correlated with right hippocampal volume. FBB retention in right occipital cortex correlated with global cognitive function.
Leinonen, 2018	14	Prospective	^{11}C-PiB and S-^{18}F-THK-5117	PET + CSF + frontal biopsy	7/14 had Aβ, 2/14 both Aβ and Ptau, and 1/14 only Ptau in biopsy. increased brain biopsy Aβ was well associated with higher PIB uptake in PET and CSF Aβ42 levels showed a strong negative correlation with PIB uptake composite score. S-[18F]-THK-5117 uptake did not show any statistically significant correlation with either brain biopsy Ptau or CSF P-tau181 or total tau.
Rinne, 2019	21	Prospective	^{11}C-PiB	PET + CSF + frontal biopsy	11/21 iNPH subjects had positive Aβ plaques through biopsy. Significant association between Aβ in the right frontal cortex biopsy specimen and PiB uptake in both right frontal cortex and whole neocortical area. 7/13 shunt responders had positive Aβ through biopsy.
Jang, 2022	114	Prospective	^{18}F-Florbetaben or ^{18}F-Flutemetamol	PET + CSF analysis	34/114 patients with NPH-like presentation had amyloid positivity. 16/34 Aβ+NPH patients responded to CSFTT and 7/16 CSFTT responders underwent shunt surgery, 5 patients experienced secondary deterioration.

Note: Aβ, β-Amyloid; Ptau, Phosphorylated Tau; PiB, Pittsburgh compound-B; HC, Healthy control.

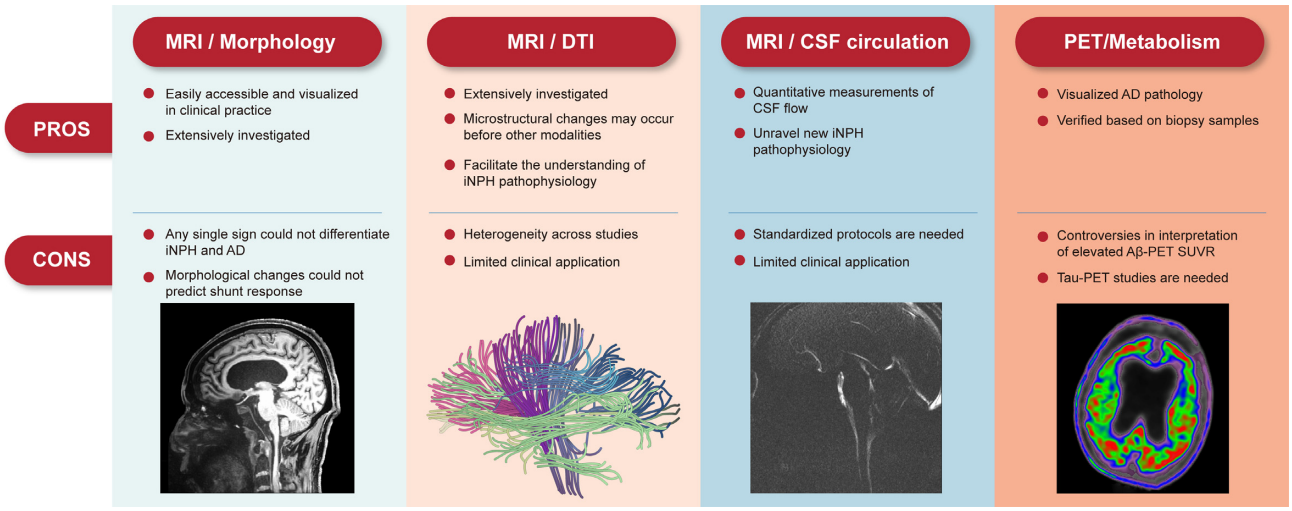

Figure 2: Pros and cons of each imaging methods for clinical evaluation of iNPH patients. Note: β, β-Amyloid; SUVR, standardized uptake value ratio.

Author contributions

H.L.C. and Y.X.Z. conceived this study and drafted the manuscript. H.L.C., Y.X.Z., H.G., K.R.H., Y.L., and Y.T.C. collected information and relevant materials. Q.C. designed the study and revised the manuscript. All coauthors revised the manuscript and approved the final version of the manuscript.

Conflicts of interest

None of the authors declare any conflicts of interest.

Acknowledgments

This work was supported by the National Natural Science Foundation of China (no. 82071203); Science and Technology Innovation 2030 "Brain Science and Brain-inspired Research" Youth Scientist Program (no. 2022ZD0213600); Natural Science Foundation of Sichuan (no. 2022NSFSC1325); and Chengdu Science and technology Bureau Program (no. 2019-YF09-00215-SN). The authors thank all participants in this study for their contributions.

References

Adams RD, Fisher CM, Hakim S, *et al.* (1965) Symptomatic occult hydrocephalus with "normal" cerebrospinal-fluid pressure. A treatable syndrome. *N Engl J Med* 117–26.

Agerskov S, Wallin M, Hellström P, *et al.* (2019) Absence of disproportionately enlarged subarachnoid space hydrocephalus, a sharp callosal angle, or other morphologic MRI markers should not be used to exclude patients with idiopathic normal pressure hydrocephalus from shunt surgery. *Am J Neuroradiol* **1**: 74–9.

Alexander AL, Hasan KM, Lazar M, *et al.* (2001) Analysis of partial volume effects in diffusion-tensor MRI. *Magn Reson Med* **5**:770–80.

Basser PJ, Mattiello J, LeBihan D (1994a) Estimation of the effective self-diffusion tensor from the NMR spin echo. *J Magn Reson, Series B* **3**:247–54.

Basser PJ, Mattiello J, LeBihan D (1994b) MR diffusion tensor spectroscopy and imaging. *Biophys J* **1**:259–67.

Bateman GA, Loiselle AM (2007) Can MR measurement of intracranial hydrodynamics and compliance differentiate which patient with idiopathic normal pressure hydrocephalus will improve following shunt insertion? *Acta Neurochir (Wien)* **5**:455–62; discussion 62.

Beaulieu C (2009) The biological basis of diffusion anisotropy. Diffusion MRI.

Benson DF, LeMay M, Patten DH, *et al.* (1970) Diagnosis of normal-pressure hydrocephalus. *N Engl J Med* **12**:609–15.

Bischof GN, Endepols H, van Eimeren T, *et al.* (2017) Tau-imaging in neurodegeneration. *Methods* 114–23.

Bloom GS (2014) Amyloid-β and tau: the trigger and bullet in Alzheimer disease pathogenesis. *JAMA Neurol* **4**:505–8.

Bradley WG Jr. (2015) CSF flow in the brain in the context of normal pressure hydrocephalus. *Am J Neuroradiol* **5**:831–8.

Bradley WG Jr., Kortman KE, Burgoyne B (1986) Flowing cerebrospinal fluid in normal and hydrocephalic states: appearance on MR images. *Radiology* **3**:611–6.

Bradley WG Jr., Scalzo D, Queralt J, *et al.* (1996) Normal-pressure hydrocephalus: evaluation with cerebrospinal fluid flow measurements at MR imaging. *Radiology* **2**:523–9.

Brix MK, Westman E, Simmons A, *et al.* (2017) The Evans' Index revisited: new cut-off levels for use in radiological assessment of ventricular enlargement in the elderly. *Eur J Radiol* 28–32.

Cabral D, Beach TG, Vedders L, *et al.* (2011) Frequency of Alzheimer's disease pathology at autopsy in patients with clinical normal pressure hydrocephalus. *Alzheimer's Dement* **5**:509–13.

Calcagni ML, Lavalle M, Mangiola A, *et al.* (2012) Early evaluation of cerebral metabolic rate of glucose (CMRglu) with 18F-FDG PET/CT and clinical assessment in idiopathic normal pressure hydrocephalus (INPH) patients before and after ventricular shunt placement: preliminary experience. *Eur J Nucl Med Mol Imaging* **2**: 236–41.

Calcagni ML, Taralli S, Mangiola A, *et al.* (2013) Regional cerebral metabolic rate of glucose evaluation and clinical assessment in patients with idiopathic normal-pressure hydrocephalus before and after ventricular shunt placement: a prospective analysis. *Clin Nucl Med* **6**:426–31.

Caligiuri ME, Quattrone A, Mechelli A, *et al.* (2022) Semi-automated assessment of the principal diffusion direction in the corpus

callosum: differentiation of idiopathic normal pressure hydrocephalus from neurodegenerative diseases. *J Neurol* **4**:1978–88.
Capone PM, Bertelson JA, Ajtai B (2020) Neuroimaging of normal pressure hydrocephalus and hydrocephalus. *Neurol Clin* **1**:171–83.
Chen J, He W, Zhang X, *et al.* (2022) Value of MRI-based semi-quantitative structural neuroimaging in predicting the prognosis of patients with idiopathic normal pressure hydrocephalus after shunt surgery. *Eur Radiol*
Chen Z, Liu C, Zhang J, *et al.* (2017) Cerebrospinal fluid Aβ42, t-tau, and p-tau levels in the differential diagnosis of idiopathic normal-pressure hydrocephalus: a systematic review and meta-analysis. *Fluids Barriers CNS* **1**:13.
Connor SE, O'Gorman R, Summers P, *et al.* (2001) SPAMM, cine phase contrast imaging and fast spin-echo T2-weighted imaging in the study of intracranial cerebrospinal fluid (CSF) flow. *Clin Radiol* **9**:763–72.
Craven CL, Toma AK, Mostafa T, *et al.* (2016) The predictive value of DESH for shunt responsiveness in idiopathic normal pressure hydrocephalus. *J Clin Neurosci* 294–8.
Daouk J, Chaarani B, Zmudka J, *et al.* (2014) Relationship between cerebrospinal fluid flow, ventricles morphology, and DTI properties in internal capsules: differences between Alzheimer's disease and normal-pressure hydrocephalus. *Acta Radiol* **8**: 992–9.
Dixon GR, Friedman JA, Luetmer PH, *et al.* (2002) Use of cerebrospinal fluid flow rates measured by phase-contrast MR to predict outcome of ventriculoperitoneal shunting for idiopathic normal-pressure hydrocephalus. *Mayo Clin Proc* **6**:509–14.
Edelman RR, Wedeen VJ, Davis KR, *et al.* (1986) Multiphasic MR imaging: a new method for direct imaging of pulsatile CSF flow. *Radiology* **3**:779–83.
Eide PK, Ringstad G (2019) Delayed clearance of cerebrospinal fluid tracer from entorhinal cortex in idiopathic normal pressure hydrocephalus: a glymphatic magnetic resonance imaging study. *J Cereb Blood Flow Metab* **7**:1355–68.
El Ahmadieh TY, Wu EM, Kafka B, *et al.* (2019) Lumbar drain trial outcomes of normal pressure hydrocephalus: a single-center experience of 254 patients. *J Neurosurg* **1**:306–12.
Engel DC, Adib SD, Schuhmann MU, *et al.* (2018) Paradigm-shift: radiological changes in the asymptomatic iNPH-patient to be: an observational study. *Fluids Barriers CNS* **1**:5.
Engel DC, Pirpamer L, Hofer E, *et al.* (2021) Incidental findings of typical iNPH imaging signs in asymptomatic subjects with subclinical cognitive decline. *Fluids Barriers CNS* **1**:37.
Evans WA (1942) An encephalographic ratio for estimating ventricular enlargement and cerebral atrophy. *AMA Arch Neurol Psychiatry* **6**:931–7.
Fleisher AS, Chen K, Quiroz YT, *et al.* (2012) Florbetapir PET analysis of amyloid-β deposition in the presenilin 1 E280A autosomal dominant Alzheimer's disease kindred: a cross-sectional study. *Lancet Neurol* **12**:1057–65.
Gaberel T, Gakuba C, Goulay R, *et al.* (2014) Impaired glymphatic perfusion after strokes revealed by contrast-enhanced MRI: a new target for fibrinolysis? *Stroke* **10**:3092–6.
Golomb J, de Leon MJ, George AE, *et al.* (1994) Hippocampal atrophy correlates with severe cognitive impairment in elderly patients with suspected normal pressure hydrocephalus. *J Neurol Neurosurg Psychiatr* **5**:590–3.
Graff-Radford NR (2014) Alzheimer CSF biomarkers may be misleading in normal-pressure hydrocephalus. *Neurology* **17**:1573–5.
Graff-Radford NR, Jones DT (2019) Normal pressure hydrocephalus. *Continuum* **1**:165–86.
Grazzini I, Venezia D, Cuneo GL (2021) The role of diffusion tensor imaging in idiopathic normal pressure hydrocephalus: a literature review. *Neuroradiology J* **2**:55–69.
Greitz D, Hannerz J, Rähn T, *et al.* (1994) MR imaging of cerebrospinal fluid dynamics in health and disease. On the vascular pathogenesis of communicating hydrocephalus and benign intracranial hypertension. *Acta Radiol* **3**:204–11.
Hashimoto M, Ishikawa M, Mori E, *et al.* (2010) Diagnosis of idiopathic normal pressure hydrocephalus is supported by MRI-based scheme: a prospective cohort study. *Cerebrospinal Fluid Res* **18**.
Hattori T, Yuasa T, Aoki S, *et al.* (2011) Altered microstructure in corticospinal tract in idiopathic normal pressure hydrocephalus: comparison with Alzheimer disease and Parkinson disease with dementia. *Am J Neuroradiol* **9**:1681–7.
Hayashi N, Matsumae M, Yatsushiro S, *et al.* (2015) Quantitative analysis of cerebrospinal fluid pressure gradients in healthy volunteers and patients with normal pressure hydrocephalus. *Neurol Med Chir* **8**:657–62.
Hiraoka K, Narita W, Kikuchi H, *et al.* (2015) Amyloid deposits and response to shunt surgery in idiopathic normal-pressure hydrocephalus. *J Neurol Sci* **1-2**:124–8.
Holodny AI, Gor DM, Watts R, *et al.* (2005) Diffusion-tensor MR tractography of somatotopic organization of corticospinal tracts in the internal capsule: initial anatomic results in contradistinction to prior reports. *Radiology* **3**:649–53.
Hong YJ, Yoon B, Shim YS, *et al.* (2010) Differences in microstructural alterations of the hippocampus in Alzheimer disease and idiopathic normal pressure hydrocephalus: a diffusion tensor imaging study. *Am J Neuroradiol* **10**:1867–72.
Horinek D, Stepan-Buksakowska I, Szabo N, *et al.* (2016) Difference in white matter microstructure in differential diagnosis of normal pressure hydrocephalus and Alzheimer's disease. *Clin Neurol Neurosurg* 52–9.
Hoza D, Vlasak A, Horinek D, *et al.* (2015) DTI-MRI biomarkers in the search for normal pressure hydrocephalus aetiology: a review. *Neurosurg Rev* **2**:239–44; discussion 44.
Iliff JJ, Lee H, Yu M, *et al.* (2013) Brain-wide pathway for waste clearance captured by contrast-enhanced MRI. *J Clin Invest* **3**:1299–309.
Iliff JJ, Wang M, Liao Y, *et al.* (2012) A paravascular pathway facilitates CSF flow through the brain parenchyma and the clearance of interstitial solutes, including amyloid β. *Sci Transl Med* **147**:147ra11.
Ishii K, Kanda T, Harada A, *et al.* (2008) Clinical impact of the callosal angle in the diagnosis of idiopathic normal pressure hydrocephalus. *Eur Radiol* **11**:2678–83.
Ishii K, Kawaguchi T, Shimada K, *et al.* (2008) Voxel-based analysis of gray matter and CSF space in idiopathic normal pressure hydrocephalus. *Dement Geriatr Cogn Disord* **4**:329–35.
Ivkovic M, Liu B, Ahmed F, *et al.* (2013) Differential diagnosis of normal pressure hydrocephalus by MRI mean diffusivity histogram analysis. *Am J Neuroradiol* **6**:1168–74.
Jack CR Jr., Wiste HJ, Lesnick TG, *et al.* (2013) Brain β-amyloid load approaches a plateau. *Neurology* **10**:890–6.
Jacobsson J, Qvarlander S, Eklund A, *et al.* (2018) Comparison of the CSF dynamics between patients with idiopathic normal pressure hydrocephalus and healthy volunteers. *J Neurosurg* 1–6.
Jagust WJ, Friedland RP, Budinger TF (1985) Positron emission tomography with [18F]fluorodeoxyglucose differentiates normal pressure hydrocephalus from Alzheimer-type dementia. *J Neurol Neurosurg Psychiatr* **11**:1091–6.
Jang H, Park SB, Kim Y, *et al.* (2018) Prognostic value of amyloid PET scan in normal pressure hydrocephalus. *J Neurol* **1**:63–73.

Jang H, Park YH, Choe YS, *et al.* (2022) Amyloid positive hydrocephalus: a hydrocephalic variant of Alzheimer's disease? *J Alzheimers Dis* **4**:1467–79.

Jang SH, Ho Kim S (2011) Diffusion tensor imaging following shunt in a patient with hydrocephalus. *J Neuroimaging* **1**:69–72.

Jaraj D, Rabiei K, Marlow T, *et al.* (2017) Estimated ventricle size using Evans index: reference values from a population-based sample. *Eur J Neurol* **3**:468–74.

Jaraj D, Rabiei K, Marlow T, *et al.* (2014) Prevalence of idiopathic normal-pressure hydrocephalus. *Neurology* **16**:1449–54.

Jeppsson A, Zetterberg H, Blennow K, *et al.* (2013) Idiopathic normal-pressure hydrocephalus: pathophysiology and diagnosis by CSF biomarkers. *Neurology* **15**:1385–92.

Jiménez-Bonilla JF, Quirce R, de Arcocha-Torres M, *et al.* (2018) (11)C-PIB retention patterns in white and grey cerebral matter in idiopathic normal pressure hydrocephalus patients. A visual analysis. *Rev Esp Med Nucl Imagen Mol* **2**:87–93.

Jurcoane A, Keil F, Szelenyi A, *et al.* (2014) Directional diffusion of corticospinal tract supports therapy decisions in idiopathic normal-pressure hydrocephalus. *Neuroradiology* **1**:5–13.

Kahlon B, Annertz M, Ståhlberg F, *et al.* (2007) Is aqueductal stroke volume, measured with cine phase-contrast magnetic resonance imaging scans useful in predicting outcome of shunt surgery in suspected normal pressure hydrocephalus? *Neurosurgery* **1**:124–30; discussion 9-30.

Kang K, Choi W, Yoon U, *et al.* (2016) Abnormal white matter integrity in elderly patients with idiopathic normal-pressure hydrocephalus: a tract-based spatial statistics study. *Eur Neurol* **1-2**:96–103.

Kang K, Yoon U, Hong J, *et al.* (2018) Amyloid Deposits and Idiopathic Normal-Pressure Hydrocephalus: An 18F-Florbetaben Study. *Eur Neurol* **79**:192–9.

Kanno S, Abe N, Saito M, *et al.* (2011) White matter involvement in idiopathic normal pressure hydrocephalus: a voxel-based diffusion tensor imaging study. *J Neurol* **11**:1949–57.

Kanno S, Saito M, Kashinoura T, *et al.* (2017) A change in brain white matter after shunt surgery in idiopathic normal pressure hydrocephalus: a tract-based spatial statistics study. *Fluids Barriers CNS* **1**:1.

Kazui H, Miyajima M, Mori E, *et al.* (2015) Lumboperitoneal shunt surgery for idiopathic normal pressure hydrocephalus (SINPHONI-2): an open-label randomised trial. *Lancet Neurol* **6**:585–94.

Kim M, Park SW, Lee JY, *et al.* (2021) Differences in brain morphology between hydrocephalus ex vacuo and idiopathic normal pressure hydrocephalus. *Psychiatry Investig* **7**:628–35.

Kim MJ, Seo SW, Lee KM, *et al.* (2011) Differential diagnosis of idiopathic normal pressure hydrocephalus from other dementias using diffusion tensor imaging. *Am J Neuroradiol* **8**:1496–503.

Kitagaki H, Mori E, Ishii K, *et al.* (1998) CSF spaces in idiopathic normal pressure hydrocephalus: morphology and volumetry. *AJNR Am J Neuroradiol* **7**:1277–84.

Klawiter EC, Schmidt RE, Trinkaus K, *et al.* (2011) Radial diffusivity predicts demyelination in ex vivo multiple sclerosis spinal cords. *Neuroimage* **4**:1454–60.

Kondo M, Tokuda T, Itsukage M, *et al.* (2013) Distribution of amyloid burden differs between idiopathic normal pressure hydrocephalus and Alzheimer's disease. *Neuroradiology J* **1**:41–6.

Korbecki A, Zimny A, Podgórski P, *et al.* (2019) Imaging of cerebrospinal fluid flow: fundamentals, techniques, and clinical applications of phase-contrast magnetic resonance imaging. *Pol J Radiol* 240–50.

Koyama T, Marumoto K, Domen K, *et al.* (2013) White matter characteristics of idiopathic normal pressure hydrocephalus: a diffusion tensor tract-based spatial statistic study. *Neurol Med Chir* **9**:601–8.

Krauss JK, Regel JP, Vach W, *et al.* (1997) Flow void of cerebrospinal fluid in idiopathic normal pressure hydrocephalus of the elderly: can it predict outcome after shunting? *Neurosurgery* **1**:67–73; discussion -4.

Leinonen V, Alafuzoff I, Aalto S, *et al.* (2008) Assessment of beta-amyloid in a frontal cortical brain biopsy specimen and by positron emission tomography with carbon 11-labeled Pittsburgh Compound B. *Arch Neurol* **10**:1304–9.

Leinonen V, Rauramaa T, Johansson J, *et al.* (2018) S-[18F]THK-5117-PET and [11C]PIB-PET imaging in idiopathic normal pressure hydrocephalus in relation to confirmed amyloid-β plaques and tau in brain biopsies. *J Alzheimers Dis* **1**:171–9.

Leinonen V, Rinne JO, Virtanen KA, *et al.* (2013) Positron emission tomography with [18F]flutemetamol and [11C]PiB for in vivo detection of cerebral cortical amyloid in normal pressure hydrocephalus patients. *Eur J Neurol* **7**:1043–52.

Lenfeldt N, Larsson A, Nyberg L, *et al.* (2011) Diffusion tensor imaging reveals supplementary lesions to frontal white matter in idiopathic normal pressure hydrocephalus. *Neurosurgery* **6**:1586–93; discussion 93.

Luetmer PH, Huston J, Friedman JA, *et al.* (2002) Measurement of cerebrospinal fluid flow at the cerebral aqueduct by use of phase-contrast magnetic resonance imaging: technique validation and utility in diagnosing idiopathic normal pressure hydrocephalus. *Neurosurgery* **3**:534–43; discussion 43-4.

Malm J, Graff-Radford NR, Ishikawa M, *et al.* (2013) Influence of comorbidities in idiopathic normal pressure hydrocephalus - research and clinical care. A report of the ISHCSF task force on comorbidities in INPH. *Fluids Barriers CNS* **1**:22.

Mantovani P, Albini-Riccioli L, Giannini G, *et al.* (2020) Anterior callosal angle: a new marker of idiopathic normal pressure hydrocephalus? *World Neurosurg* e548–52.

Mantovani P, Giannini G, Milletti D, *et al.* (2021) Anterior callosal angle correlates with gait impairment and fall risk in iNPH patients. *Acta Neurochir* **3**:759–66.

Mataró M, Matarín M, Poca MA, *et al.* (2007) Functional and magnetic resonance imaging correlates of corpus callosum in normal pressure hydrocephalus before and after shunting. *J Neurol Neurosurg Psychiatry* **4**:395–8.

Medina DA, Gaviria M (2008) Diffusion tensor imaging investigations in Alzheimer's disease: the resurgence of white matter compromise in the cortical dysfunction of the aging brain. *Neuropsychiatr Dis Treat* **4**:737–42.

Miskin N, Patel H, Franceschi AM, *et al.* (2017) Diagnosis of normal-pressure hydrocephalus: use of traditional measures in the era of volumetric MR imaging. *Radiology* **1**:197–205.

Moore DW, Kovanlikaya I, Heier LA, *et al.* (2012) A pilot study of quantitative MRI measurements of ventricular volume and cortical atrophy for the differential diagnosis of normal pressure hydrocephalus. *Neurol Res Int* 718150.

Mori E, Ishikawa M, Kato T, *et al.* (2012) Guidelines for management of idiopathic normal pressure hydrocephalus: second edition. *Neurol Med Chir* **11**:775–809.

Moura LM, Luccas R, de Paiva JPQ, *et al.* (2019) Diffusion tensor imaging biomarkers to predict motor outcomes in stroke: a narrative review. *Front Neurol* 445.

Nakajima M, Yamada S, Miyajima M, *et al.* (2021) Guidelines for management of idiopathic normal pressure hydrocephalus (third edition): endorsed by the Japanese Society of Normal Pressure Hydrocephalus. *Neurol Med Chir* **2**:63–97.

Narita W, Nishio Y, Baba T, *et al.* (2016) High-convexity tightness predicts the shunt response in idiopathic normal pressure hydrocephalus. *Am J Neuroradiol* **10**:1831–7.

Ossenkoppele R, Smith R, Mattsson-Carlgren N, *et al.* (2021) Accuracy of tau positron emission tomography as a prognostic marker in preclinical and prodromal Alzheimer disease: a head-to-Head comparison against amyloid positron emission tomography and magnetic resonance imaging. *JAMA Neurol* **8**: 961–71.

Park HY, Kim M, Suh CH, *et al.* (2021) Diagnostic performance and interobserver agreement of the callosal angle and Evans' index in idiopathic normal pressure hydrocephalus: a systematic review and meta-analysis. *Eur Radiol* **7**:5300–11.

Pomeraniec IJ, Bond AE, Lopes MB, *et al.* (2016) Concurrent Alzheimer's pathology in patients with clinical normal pressure hydrocephalus: correlation of high-volume lumbar puncture results, cortical brain biopsies, and outcomes. *J Neurosurg* **2**:382–8.

Rasmussen MK, Mestre H, Nedergaard M (2018) The glymphatic pathway in neurological disorders. *Lancet Neurol* **11**:1016–24.

Rekate HL, Nadkarni TD, Wallace D (2008) The importance of the cortical subarachnoid space in understanding hydrocephalus. *J Neurosurg Pediatrics* **1**:1–11.

Relkin N, Marmarou A, Klinge P, *et al.* (2005) Diagnosing idiopathic normal-pressure hydrocephalus. *Neurosurgery* **3** Suppl:S4-16; discussion ii-v.

Ringstad G, Emblem KE, Eide PK (2016) Phase-contrast magnetic resonance imaging reveals net retrograde aqueductal flow in idiopathic normal pressure hydrocephalus. *J Neurosurg* **6**:1850–7.

Ringstad G, Valnes LM, Dale AM, *et al.* (2018) Brain-wide glymphatic enhancement and clearance in humans assessed with MRI. *JCI Insight* 13.

Ringstad G, Vatnehol SAS, Eide PK (2017) Glymphatic MRI in idiopathic normal pressure hydrocephalus. *Brain* **10**:2691–705.

Rinne JO, Frantzen J, Leinonen V, *et al.* (2014) Prospective flutemetamol positron emission tomography and histopathology in normal pressure hydrocephalus. *Neurodegener Dis* **13**:237–45 .

Rinne JO, Suotunen T, Rummukainen J, *et al.* (2019) [11C]PIB PET Is Associated with the Brain Biopsy Amyloid-β Load in Subjects Examined for Normal Pressure Hydrocephalus. *J Alzheimers Dis* **67**:1343–1351 .

Rinne JO, Wong DF, Wolk DA, *et al.* (2012) [(18)F]Flutemetamol PET imaging and cortical biopsy histopathology for fibrillar amyloid β detection in living subjects with normal pressure hydrocephalus: pooled analysis of four studies. *Acta Neuropathol* **6**:833–45.

Röricht S, Meyer BU, Woiciechowsky C, *et al.* (1998) Callosal and corticospinal tract function in patients with hydrocephalus: a morphometric and transcranial magnetic stimulation study. *J Neurol* **5**:280–8.

Rose SE, Janke AL, Chalk JB (2008) Gray and white matter changes in Alzheimer's disease: a diffusion tensor imaging study. *J Magn Reson Imaging* **1**:20–6.

Savolainen S, Laakso MP, Paljärvi L, *et al.* (2000) MR imaging of the hippocampus in normal pressure hydrocephalus: correlations with cortical Alzheimer's disease confirmed by pathologic analysis. *AJNR Am J Neuroradiol* **2**:409–14.

Scheel M, Diekhoff T, Sprung C, *et al.* (2012) Diffusion tensor imaging in hydrocephalus—findings before and after shunt surgery. *Acta Neurochir* **9**:1699–706.

Schmahmann JD, Pandya DN (2006) *Fiber Pathways of the Brain*. Oxford University Press.

Scollato A, Tenenbaum R, Bahl G, *et al.* (2008) Changes in aqueductal CSF stroke volume and progression of symptoms in patients with unshunted idiopathic normal pressure hydrocephalus. *Am J Neuroradiol* **1**:192–7.

Shokri-Kojori E, Wang GJ, Wiers CE, *et al.* (2018) β-Amyloid accumulation in the human brain after one night of sleep deprivation. *Proc Natl Acad Sci USA* **17**:4483–8.

Siasios I, Kapsalaki EZ, Fountas KN, *et al.* (2016) The role of diffusion tensor imaging and fractional anisotropy in the evaluation of patients with idiopathic normal pressure hydrocephalus: a literature review. *Neurosurg Focus* **3**:E12.

Skalický P, Mládek A, Vlasák A, *et al.* (2020) Normal pressure hydrocephalus-an overview of pathophysiological mechanisms and diagnostic procedures. *Neurosurg Rev* **6**:1451–64.

Takeuchi T, Goto H, Izaki K, *et al.* (2007) Pathophysiology of cerebral circulatory disorders in idiopathic normal pressure hydrocephalus. *Neurol Med Chir* **7**:299–306; discussion

Takizawa K, Matsumae M, Hayashi N, *et al.* (2017) Hyperdynamic CSF motion profiles found in idiopathic normal pressure hydrocephalus and Alzheimer's disease assessed by fluid mechanics derived from magnetic resonance images. *Fluids Barriers CNS* **1**:29.

Tan C, Wang X, Wang Y, *et al.* (2021) The pathogenesis based on the glymphatic system, diagnosis, and treatment of idiopathic normal pressure hydrocephalus. *Clin Interv Aging* 139–53.

Tedeschi E, Hasselbalch SG, Waldemar G, *et al.* (1995) Heterogeneous cerebral glucose metabolism in normal pressure hydrocephalus. *J Neurol Neurosurg Psychiatry* **6**:608–15.

Teipel S, Grothe MJ, Zhou J, *et al.* (2016) Measuring cortical connectivity in Alzheimer's disease as a brain neural network pathology: toward clinical applications. *J Int Neuropsychol Soc* **2**:138–63.

Thavarajasingam SG, El-Khatib M, Rea M, *et al.* (2021) Clinical predictors of shunt response in the diagnosis and treatment of idiopathic normal pressure hydrocephalus: a systematic review and meta-analysis. *Acta Neurochir* **10**:2641–72.

Toma AK, Holl E, Kitchen ND, *et al.* (2011) Evans' Index revisited: the need for an alternative in normal pressure hydrocephalus. *Neurosurgery* **4**:939–44.

Townley RA, Botha H, Graff-Radford J, *et al.* (2018) (18)F-FDG PET-CT pattern in idiopathic normal pressure hydrocephalus. *NeuroImage: Clinical* 897–902.

Uluğ AM, Truong TN, Filippi CG, *et al.* (2003) Diffusion imaging in obstructive hydrocephalus. *AJNR Am J Neuroradiol* **6**:1171–6.

Virhammar J, Laurell K, Cesarini KG, *et al.* (2014) Preoperative prognostic value of MRI findings in 108 patients with idiopathic normal pressure hydrocephalus. *Am J Neuroradiol* **12**:2311–8.

Wagshul ME, Chen JJ, Egnor MR, *et al.* (2006) Amplitude and phase of cerebrospinal fluid pulsations: experimental studies and review of the literature. *J Neurosurg* **5**:810–9.

Wagshul ME, Eide PK, Madsen JR (2011) The pulsating brain: a review of experimental and clinical studies of intracranial pulsatility. *Fluids Barriers CNS* **1**:5.

Wang Z, Zhang Y, Hu F, *et al.* (2020) Pathogenesis and pathophysiology of idiopathic normal pressure hydrocephalus. *CNS Neurosci Ther* **12**:1230–40.

Winston GP (2012) The physical and biological basis of quantitative parameters derived from diffusion MRI. *Quant Imaging Med Surg* **4**:254–65.

Wolk DA, Grachev ID, Buckley C, *et al.* (2011) Association between in vivo fluorine 18-labeled flutemetamol amyloid positron emission tomography imaging and in vivo cerebral cortical histopathology. *Arch Neurol* **11**:1398–403.

Wong DF, Moghekar AR, Rigamonti D, *et al.* (2013) An in vivo evaluation of cerebral cortical amyloid with [18F]flutemetamol using positron emission tomography compared with parietal biopsy

samples in living normal pressure hydrocephalus patients. *Mol Imaging Biol* **2**:230–7.

Yamada S, Ishikawa M, Yamamoto K (2016) Comparison of CSF distribution between idiopathic normal pressure hydrocephalus and Alzheimer disease. *Am J Neuroradiol* **7**:1249–55.

Yamada S, Ishikawa M, Yamamoto K (2015) Optimal diagnostic indices for idiopathic normal pressure hydrocephalus based on the 3D quantitative volumetric analysis for the cerebral ventricle and subarachnoid space. *Am J Neuroradiol* **12**:2262–9.

Yamada S, Tsuchiya K, Bradley WG, *et al.* (2015) Current and emerging MR imaging techniques for the diagnosis and management of CSF flow disorders: a review of phase-contrast and time-spatial labeling inversion pulse. *Am J Neuroradiol* **4**: 623–30.

Yamamoto D, Kazui H, Wada T, *et al.* (2013) Association between milder brain deformation before a shunt operation and improvement in cognition and gait in idiopathic normal pressure hydrocephalus. *Dement Geriatr Cogn Disord* **3-4**: 197–207.

Yamashita F, Sasaki M, Saito M, *et al.* (2014) Voxel-based morphometry of disproportionate cerebrospinal fluid space distribution for the differential diagnosis of idiopathic normal pressure hydrocephalus. *J Neuroimaging* **4**:359–65.

Yamashita F, Sasaki M, Takahashi S, *et al.* (2010) Detection of changes in cerebrospinal fluid space in idiopathic normal pressure hydrocephalus using voxel-based morphometry. *Neuroradiology* **5**:381–6.

Younes K, Hasan KM, Kamali A, *et al.* (2019) Diffusion tensor imaging of the superior thalamic radiation and cerebrospinal fluid distribution in idiopathic normal pressure hydrocephalus. *J Neuroimaging* **2**:242–51.

Zhou B, Zuo YX, Jiang RT (2019) Astrocyte morphology: diversity, plasticity, and role in neurological diseases. *CNS Neurosci Ther* **6**:665–73.